DYNAMIC BEHAVIOR OF VERTICAL CYLINDER DUE TO WAVE FORCE

Toru Sawaragi* and Takayuki Nakamura**

ABSTRACT

This paper describes the dynamic behavior of a fixed cylindrical pile due to both the in-line or longitudinal force and lift or transverse force in regular waves. Resonant response of the pile due to the lift force in the direction normal to the wave propagation direction is discovered at the period ratios of T_w/T_n=2,3,4,5 and 6 (T_w : the wave period, T_n : the natural period of the pile). Furthermore, the resonant responses in the wave propagation direction due to the in-line force also appear at the same period ratios, in addition to the well known resonance point of T_w/T_n=1. Moreover, dynamic displacements of the pile in the direction normal to the wave propagation direction are longer than those in the wave propagation direction when the period ratio is longer than 1.6 and Keulegan-Carpenter number is larger than 6.

Next, for the purpose of the ocean structural design, the methods of estimating the dynamic displacements in both directions and of estimating the dynamic displacements considering both are derived by using Morison's equation and lift force equation formulated bythe authors. The displacements calculated are compared exactly with the experimental results to investigate the validity of the proposed method.

INTRODUCTION

In recent studies of wave force on a cylindrical pile, it has been discovered that a lift force acts on the pile in the direction normal to the wave propagation direction, in addition to a in-line force acting on the pile, as described by Morison's equation, in the wave propagation direction.

It was pointed out by Bidde[1],Sarpkaya[2] and the authors[3] that the lift force has a magnitude as large as the in-line force, and that the frequency of the lift force is higher than that of the wave and the in-line force. On the other hand, considering the fact that the natural frequency (f_n) is generally higher than the wave frequency (f_w), the lift force may be important when the resonance response of a fixed off-shore structure in waves is examined. In fact, Wiegel et al[4] reported that 2-foot pile vibrates largely with the vibration period of 2.5 seconds in the direction normal to the wave propagation direction due to the alternate breaking of the large vortices under the large wave condition with the wave period being about 13 seconds. And they also reported that the test pile was broken by the latteralvibration described above.

With the above-described background, first, in this paper, the influence of lift force on the dynamic response of a cylindrical pile of cantilever type was investigated by experiments, and the effects of a period ratio (T_w/T_n) or a frequency ratio (f_w/f_n) and Keulegan-Carpenter number for the dynamic response are discussed. (T_w: the wave period and

*Professor, Department of Civil Engneering, Suita, Osaka,565, Japan
**Assistant Professor, Department of Ocean Engineering, Ehime, Japan

equal to $1/f_w$, T_n: the natural period of the pile and equal to $1/f_n$).

Secondly, in order to estimate the dynamic response in the in-line and normal direction, equations on dynamic displacements in two directions are derived by using the Morison's equation on the in-line force and the lift force equation formulated by the authors. Furthermore, the combined dynamic displacement is calculated, and these calculated results are compared with the experimental results.

EXPERIMENT

The wave tank used in this experiment was a 0.7m wide, 0.95m deep and 30m long wave channel at the Hydraulics Laboratory of Civil Engineering, Osaka University. A flap type wave generator was located at one end of the wave tank and a pebble beach was installed at the other end of the wave tank to absorb the wave energy.

Model cylinders used in this experiment were two kinds of cantilever type structure with a concentrated mass at its top as shown schematically in Fig. 1(A) and (B). Each model pile consisted of three parts, i.e., a concentrated mass, a circular cylinder and a spring bar. The mass was made of steel and had the same diameter as that of the cylinder. The spring bar was also made of steel and had a circular cross section with diameter of 5.5mm for the model pile of Fig. 1(A) and 5.9mm for that of Fig. 1(B). The model pile of Fig. 1(A)was fixed on the shelf in the square box made of steel with the same height as that of the horizontal flat bed. In this case, a 2.5cm cylinder made of arcylicresin was used for a circular cylinder and the water depth was kept constant at 35cm above the horizontal bed. On the other hand, the model pile of Fig. 1(B) was fixed on the channel-shaped steel having a height of 5cm that was rigidly connected to the bottom of the wave tank. In this case, a 3cm cylinder was used and the depth of the water was kept constant at 65cm above the bottom of the wave tank. The model pile of Fig. 1(A) was used only for the purpose of measuring the dynamic response in the comparatively small ranges of T_W/T_n and the one of Fig. 1(B) was used for that of T_W/T_n being large.

In this experiment, five kinds of concentrated mass were mounted on these model piles, considering the efficiency of the wave generator and values of period ratio(T_W/T_n). The values of these masses are tabulated in Table 1(A) and (B) for the model pile of Fig. 1(A) and (B) respectively. In this table, the natural period T_n and the natural frequency f_n of the pile measured from the experiment of free vibration in water, and the logarithmic decrement δ measured from the experiment of free vibration in air are also tabulated for each mass.

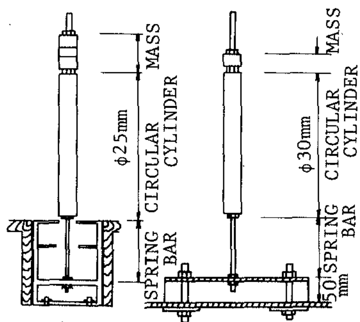

(A) (B)

Fig. 1 Structural model of experimental cylinders

In order to clarify the effects of Keulegan-Carpenter number and the period or frequency ratio on the dynamic response of the model pile, the region of the model ratio (T_w/T_n) wave fixed between 0.8 and 7.5, and the range of rmsK-C number (rms K-C), which is the root mean square value of Keulegan-Carpenter number at each vertical elevation of the cylinder, was from 2 to 20. The range of rms Reynolds number (rmsRe), which is the root mean square value of Reynolds number at each vertical elevation of the cylinder, was from about 2000 to 8000.

EXP. CYL.	mass (g)	T_n (sec)	f_n (Hz)	δ
(A)	0.276	0.504	1.984	0.040
	0.599	0.740	1.351	0.043
	0.914	0.930	1.075	0.045
(B)	0	0.298	3.356	0.993
	0.142	0.386	2.591	0.053

Table 1 Dynamic characteristic of the model pile

The wave condition used in this study was as follows, the wave height was fixed between 2cm and 16cm, and that of the wave period was 0.6sec to 2.3sec.

In this experment, a 16-mm cine-camera was located right above the pile to measure the dynamic displacement at the top of it. Also the strain gages were mounted near the fixed end of the cantilever to measure the dynamic overturning moment in both directions. The wave gage used was a parallel-wire resistance type and was installes at the side of the model pile. Furthermore, in order to synchronize the 16mm-movie record with records of water surface elevation and dynamic moment, pulse signals of 10 Hz were utilized. The movie records were analyzed with an electronic gragh-pen system, and then locus of the top of the model pile was reproduced with a graphic display system.

DYNAMIC BEHAVIOR OF THE MODEL PILE

1) DYNAMIC LOCUS OF THE MODEL PILE

Typical loci of the top of the model pile during one wave cycle of the incident wave (except (B-1)) are shown schematically in Fig.2 with the frequency ratio as a parameter. In Fig. 2, the X-axis is the direction of the wave propagation direction and Y-axis is the direction normal to the wave propagation direction. From this figure, the following results are appeared. (A) : In the range of frequency ratio (f_w/f_n) larger than 0.9 (Fig. 2 (A-1) ~ (A-3)), the displacement of the top of the pile in the X direction is predominant in comparison with that in the Y direction and the locus shows a nealy straight line in the X direction. Because of the well-known resonance at f_w/f_n=1 due to the in-line force, the pile vibrates largely in the X direction. In this case, the frequencies of the displacements in both directions possess the wave frequency as shown in Fig. 3 (A). Here, Fig. 3 shows the time histories of the displacements in both directions and corresponds to the locus shown in Fig. 2, respectively. (B) : In the range of frequency ratio ranging from 0.6 to 0.9, the locus looks line a letter of infinity sign (∞), as shown in Fig. 2 (B-1) and (B-2). In this case, the Y-displacement has the second harmonic frequency, as shown in Fig. 3 (B), but the X-displacement has only the wave frequency. (C) ; When the frequency ratio ranges from 0.4 to 0.6, the locus is nearly a double ellipse as shown in Fig. 2 (C-1) and (C-2). In this case , the Y-displacement is much greater than the X displacement,

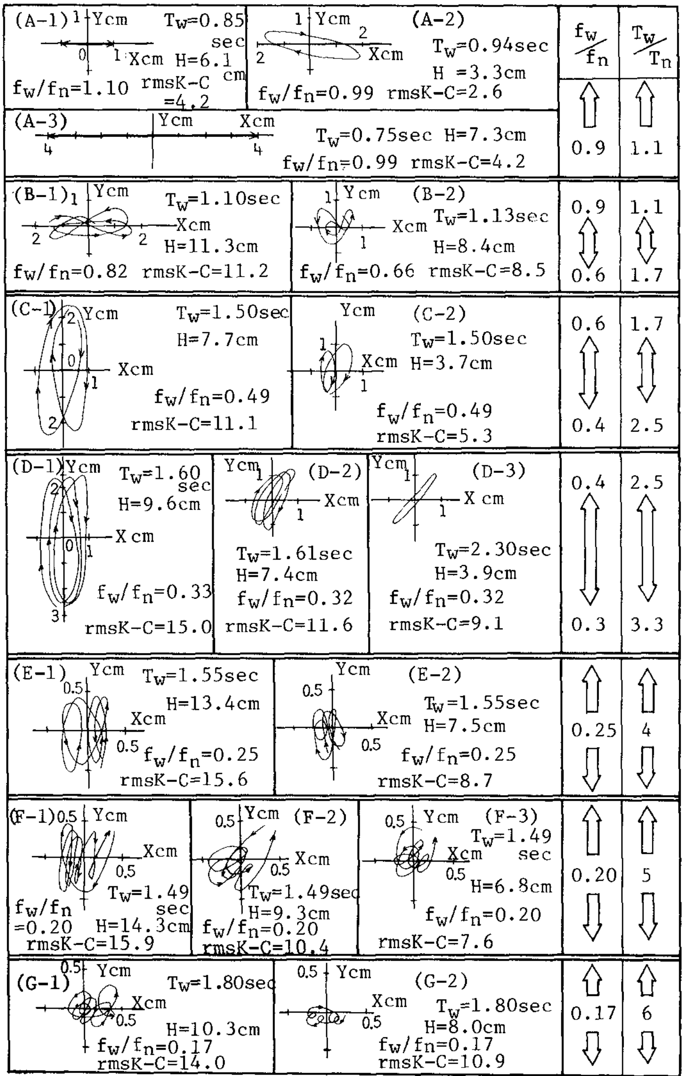

Fig.2 Loci of dynamic displacements at the top of the cylinder

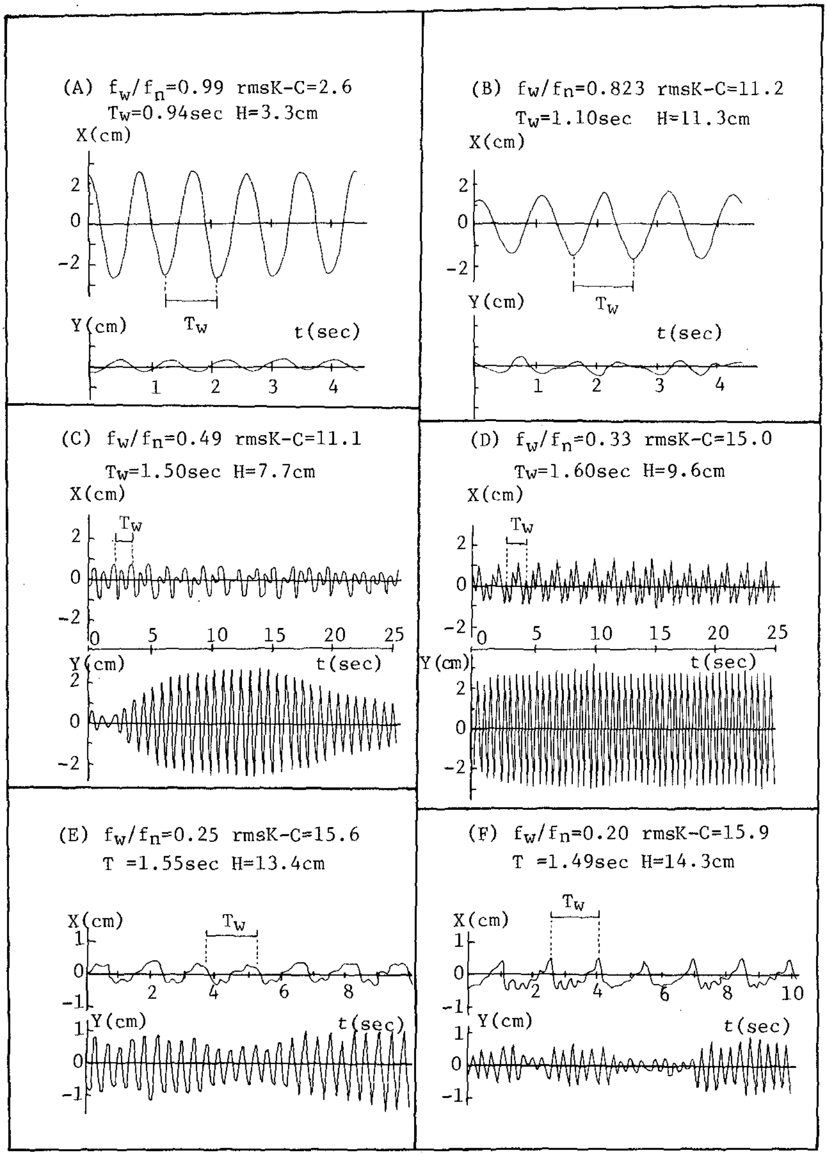

Fig. 3 Time history of the X and Y displacement

because the pile is resonanted by the lift force component with the frequency two times as large as the wave frequency. Consequently, the Y displacement vibrates largely with the second harmonic frequency of the wave as shown in Fig. 3 (C). On the other hand, the X displacement has both the wave frequency and the second harmonic frequency of the wave. Since the characteristics of the lift force frequency will be given later, readers may want to refer to Fig. 6. (D) : With a frequency ratio ranging from 0.3 to 0.4 the locus shows a long ellipse and a triple ellipse as shown in Fig.2 (D-1), (D-2) and (D-3). In this case, the pile is resonanted at $f_w/f_n=1/3$ by the lift force component which corresponds to the third harmonic frequency of the wave. Therefore, the Y displacement vibrates largely with the frequency as shown in Fig. 3 (D). From this figure, it can be seen that the X displacement has also the third harmonic frequency of the wave in addition to the wave frequency, and like the case of (C), the Y displacement is larger than the X displacement. (E) : When the frequency ratio is nearly equal to 0.25, the locus is similar to the figure of a tetra ellipse and the Y-displacement has also the more significant magnitude compared with the X displacement (see Fig. 3(E)). Furthermore, the smaller the value of the frequency ratio, as shown in Fig. 2 (F-1), (F-2),(F-3), (G-1) and (G-2), the more complicated the dynamic locus becomes owing to the appearance of higher harmonic frequency components in both displacements, and in the range of frequency ratio nearly equal to 1/5 and 1/6, it can be seen that the Y displacement cannot be neglected in comparison with the X displacement. Here, the effect of rmsK-C on the locus is not clearly distinguishable, but the following features may be pointed out: when the frequency ratio nearly equals 1, the Y displacement appears only at comparatively small values of rmsK-C, and in the range of frequency ratio smaller than 0.9, the Y displacement decreases with decreasing values of rmsK-C and the Y displacement is equal to or smaller than the X displacement when the value of rmsK-C is comparatively small.

The reason for the higher harmonic frequency of the wave of the X displacement will be presented later.

2) RESONANT CHARACTERISTICS OF THE PILE

In order to examine the resonant characteristics of the pile due to the in-line and lift forces, the resonant curves in both directions were obtained. Fig. 4 and Fig. 5 show the resonant curves in the X and Y directions respectively with rmsK-C as a parameter. In these figures, the abscissa is the period ratio $(1/(f_w/f_n))$ and the ordinate is the so-called amplification ratio, i.e. the ratio of the dynamic displacement to the static displacement due to the wave forces. Here, the static displacements, X_s and Y_s, are calculated by means of the structural model shown in Fig. 9, and by using the Morison's equation on the in-line force and the lift force equation (Eq. 7) derived by the authors on the lift force. The linear wave theory is also used. The wave force is integrated from the bottom of the circular cylinder to the elevating water surface as a sinusoidal wave. In these figures, $X_{p1/10}$ and $Y_{p1/10}$ are meausred one-tenth maximum dynamic displacements of X and Y respectively, since the Y displacement was irregular in regular waves as shown in Fig. 3.

From Fig. 4, it is clear that the resonant response due to a in-line

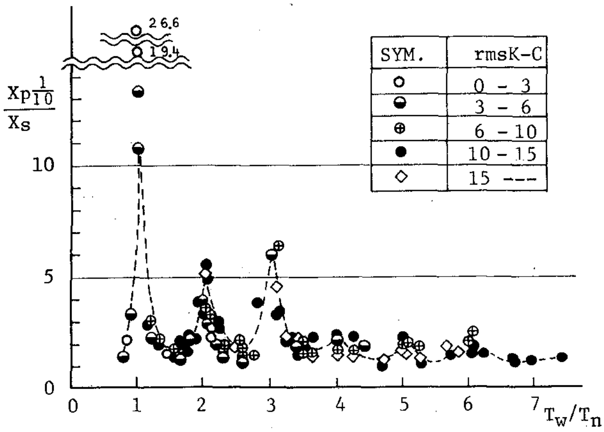

Fig.4 amplification ratio in X-direction

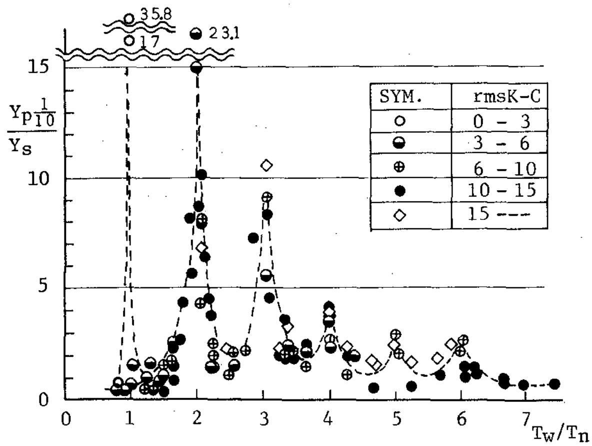

Fig.5 Amplification ratio in Y-direction

force appears at the period ratios T_w/T_n =1,2,3,4,5 and 6, but there is no response at the period ratio T_w/T_n =7. Among these resonances, the well-known resonance at T_w/T_n=1 is the most predominant, but the resonance at the period ratio T_w/T_n =2 and 3 are also comparatively large.

The reason for the appearance of the response at T_w/T_n=2 and 3 may be due to the fact that the in-line force (Fx) and the over-turning moment (M_x) caused by the in-line force have higher frequency components than the wave based on the non-linearity of the drag force and the finite amplitude nature of the water wave. A good example illustrating this fact is presented in Table 2. This table shows the result of a harmonic analysis of F_x and M_x acting on a vertical circular cylinder in waves during one wave cycle. Here F_x and M_x are calculated by using the Morison's equation and the linear wave theory. Table 2 (I) is the result of the consideration of the effect of the finite amplitude nature, the wave force still being considered as a sinusoidal wave, i.e. the integral region of the wave force is from the bottom of the circular cylinder to the elevating water surface. On the other hand, Table 2 (II) indicates the result of neglecting the above-described effect. It is seen that F_x and M_x have higher harmonics than the wave frequency as shown in Table 2 (I) and (II). Moreover, it is clear that these components with the second harmonic frequency of the wave differ significantly between (I) and (II), but this significant difference between (I) and (II) cannot be seen when n=3. The non-linearity of the

	nf_w	(I)	(II)
F_X	n=1	18.46×10^{-3} (Kg)	18.38×10^{-3} (Kg)
	2	1.63	0.10
	3	2.13	2.08
	4	0.06	0.10
	5	0.31	0.31
	6	0.08	0.10
M_X	n=1	353.63×10^{-3} (Kg cm)	348.25×10^{-3} (Kg cm)
	2	56.03	1.89
	3	43.96	40.98
	4	3.76	1.89
	5	5.84	6.15
	6	1.29	1.89
T=1.5sec H=8cm rmsK-C=11.53 D=2.5cm			

Table 2 Harmonic anlysis of F_X and M_X

drag force and the effect of the finite amplitude nature of the water wave on the dynamics of the pile will be described later on in detail.

From Fig. 5, it is evident that the resonant response due to the lift force appears at the same period ratios as those in the X direction. In this case, however, the resonant condition depends on rmsK-C, i.e. the resonance at $T_w/T_n=1$ is predominant for values of rmsK-C smaller than 3, and the resonances at $T_w/T_n=2$ and 3 are the most predominant in case of rmsK-C being larger than 3. It may be considered that these facts have a close relation with the frequency characteristics of a lift force and the magnitude as shown in Fig. 6 and 7。 Fig. 6 shows the variation of the predominant non-dimensional lift energy ($S_L(nf_w)\Delta f/\sigma^2{}_L$, n=1-4) for each harmonic component of the wave frequency with rmsK-C. This figure was obtained by using the experimental result of the wave force on a rigidly supported vertical circular cylinder and was presented in Ref.(3), too. Here, $S_L(nf_w)\Delta f$ is the lift energy for the n-th harmonic of the wave frequency, and $\sigma^2{}_L$ is the variance of the lift force. From this figure, it can be seen that the predominant lift frequency equals the wave frequency in the range where rmsK-C is smaller than 3 approximately, corresponds to the second harmonic frequency of the wave in the rmsK-C range of 6 to 12, and equals the third harmonic frequency of the wave in the range of rmsK-C larger than 13, and the rest is the transition region from f_w to $2f_w$ and from $2f_w$ to $3f_w$. Fig. 7 shows the ratio of the one-tenth maximum lift force ($F_{L1/10}$) to the mean value of the maximum in-line forces (F_{Tm}) with rmsK-C as a parameter, and this figure was obtained by using the same experimental results described above. Furthermore, the experimental results of Sarpkaya[5], using the U-shaped water-tunnel, are given by the dotted line in Fig. 7. From this figure, the magnitude of the lift force increases rapidly as compared with the in-line force as rmsK-C increases(from 5 to 10) and it reaches the maximum value of 1.1 times the in-line force at rmsK-C=10.

Therefore, from the characteristics of the lift force described above, it can be considered that the resonance at $T_w/T_n=1$ in the Y-direction appears only when rmsK-C is lower than 3, due to the predominant lift force component having the waver frequency(see Fig. 6)。 However, this resonance can be neglected as shown later, because the magnitude of the lift force is comparatively smaller than that of the in-line force when rmsK-C is smaller than 3 as shown in Fig. 7, and the dynamic displacement in the Y-direction is very small compared with that in the X-direction at this period ratio. Furthermore, at T_w/T_n=2, the resonant response appears only when rmsK-C is larger than 3, due to the predominant second harmonic frequency shown in Fig. 6. From the investigation described above, it can be concluded that the resonant characteristics of the pile due to both the in-line and the lift force have a close relation to the charcteristics of the wave forces, including the frequency and magnitude of the wave force.

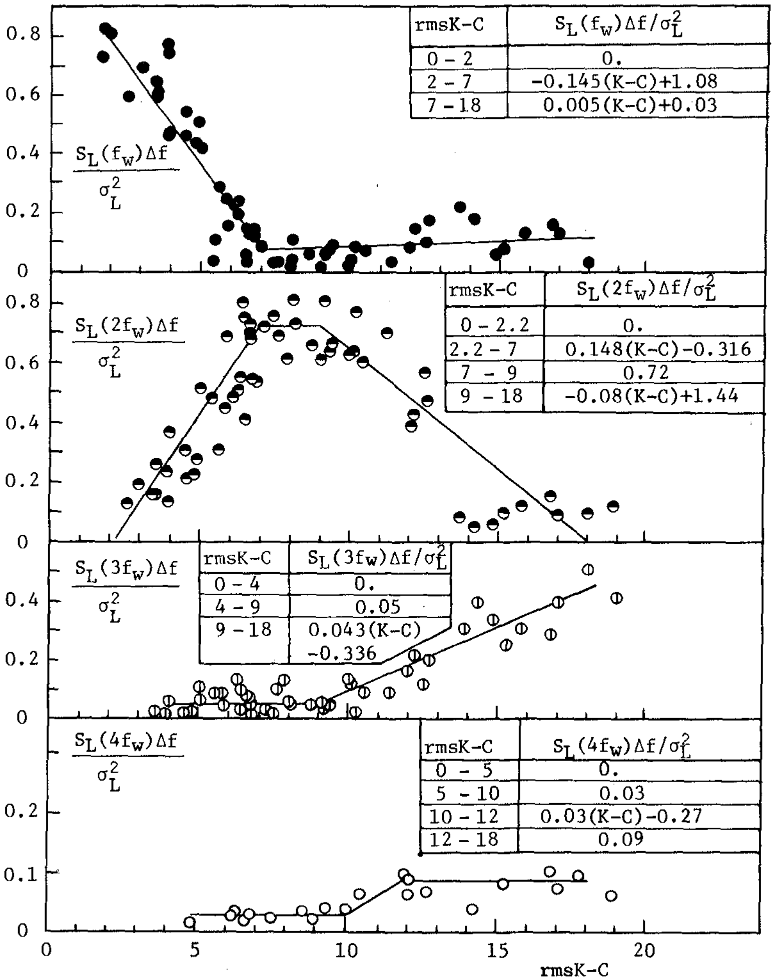

Fig. 6 Predominant lift energy versus rmsK-C

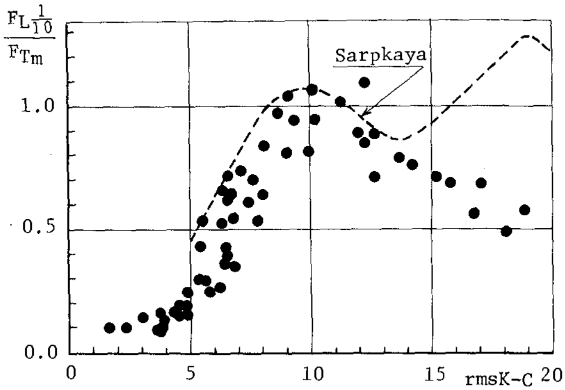

Fig. 7 Ratio of maximum one-tenth lift force to in-line force versus rmsK-C

3) MAGNITUDE OF THE Y-DISPLACEMENT

From the practical point of view, it may be important to know the magnitude of the Y-displacement in relation to the X-displacement. Fig. 8 shows the variation of the ratio of the Y-displacement to the X-displacement in terms of T_w/T_n. Here, the one-tenth maximum displacements in both directions are used. From this figure, it is clear that the X-displacement is predominant when the period ratio is smaller than 1.5 approximately. On the other hand, the Y-displacement is predominant in the range where the period ratio is larger than 1.5 and especially the predominance of the Y-displacement is conspicuous near the resonance points described above except at $T_w/T_n=1$, when rmsK-C is larger than 6. This reason can be given by the characteristics of the lift force as shown in Fig. 6 and Fig. 7.

Therefore, from the above-mentioned experimental results, it can be pointed out that rather than a in-line force, a lift force is the more significant force when the natural period of the structure is lower than the wave period and rmsK-C is higher than 6.

ESTIMATION OF DYNAMIC RESPONSE

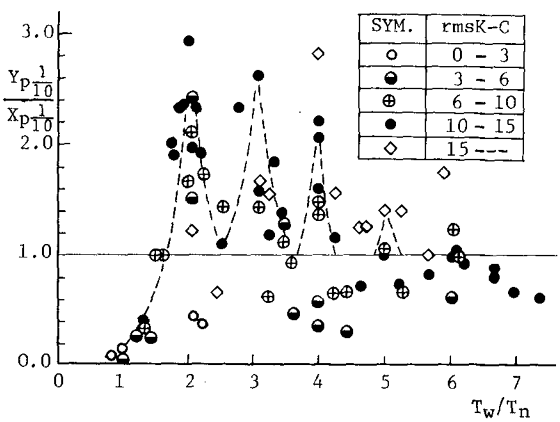

Fig. 8 Ratio of Y-displacement to X-displacement versus period ratio

1) FORMULATION OF THE LIFT FORCE EQUATION

As mentioned above, the computation of a lift force is necessary in order to estimate the dynamic response of a structure due to it. However, it is difficult to formulate the lift force equation which can express the time variation of the lift force, because the lift force is generated by the alternate breaking of the eddies and it is irregular even in regular waves. Therefore,

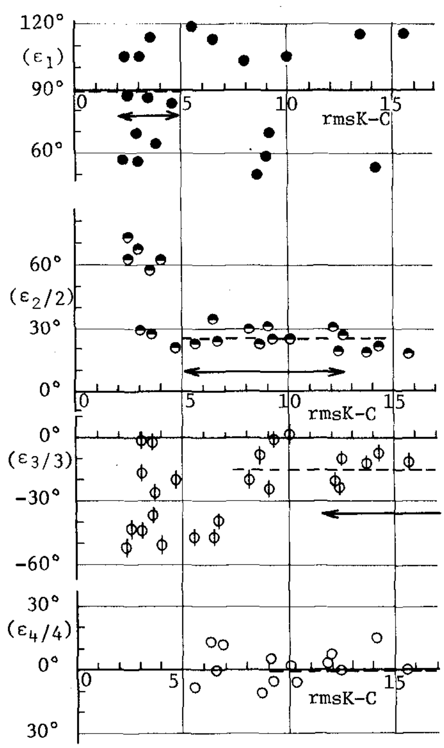

Fig. 9 Phase angle of the n-th harmonic lift force

the formulation of the lift force is performed empirically based on the experimental result of wave forces on a rigidly supported vertical circular cylinder.

It may be assumed that the formula is expressed by the superposition of each predominant frequency component of the lift force as shown in Fig. 6, given by Eq.(1).

$$f_L(t)=\sigma_L \sum_{n=1}^{4} \sqrt{\frac{2S_L(nf_w)\Delta f}{\sigma_L^2}} \times \cos(2n\pi f_w t-\varepsilon_n) \qquad (1)$$

Here, $f_L(t)$:the lift force per unit length; $S_L(nf_w)$:the variance of the lift force; and ε_n:the phase angle between the n-th harmonic lift force component and the incident wave. The spectral energy of the n-th harmonic lift force may be given by the experimental result of Fig. 6. In this study, the non-dimensional n-th harmonic lift force energy is given by the empirical formula which is specified at the right side of Fig. 6, and it is shown by the solid line in this figure. Further, the phase angle was obtained by using the result of harmonic analysis of both the measured lift force and wave records. The change of phase angle with rms K-C is shown in Fig.9, in which the predminant region of the n-th harmonic lift force is also shown by an arrow mark. The scattering of the experimental results is relatively large, but if attention is focussed on each predominant region ε_n may be considered as a constant value, i.e. $\varepsilon_2/2=25°$, $\varepsilon_3/3=-15°$ and $\varepsilon_4/4=0°$. However, as ε_1 is scattered from 60° to 120° in the predominant region of f_w frequency, it seems to be quite all right to consider that the average value of ε_1 is 90°, because the magnitude of the lift force is quite small in comparison with the in-line force in the region where rmsK-C is smaller than 5, as shown in Fig. 7.

On the other hand, Chakrabalti et al[6] have presented the lift force as shown in Eq. 2.

$$f_L(t)=\frac{1}{2}\rho D U_m^2 \sum_{n=1}^{4} C_{Ln}\sin(2n\pi f_w t-\sigma_n) \qquad (2)$$

Here, U_m : the maximum horizontal water particle velocity; C_{Ln} : the lift coefficient for the n-th harmonic lift force; D : the diamter of a circular cylinder; and ρ : the dencity of water.

Since the lift force in regular waves is irregular, $f_L(t)$ is considered as a random function of time. With the exception of C_{Ln}, the terms on the right hand side of Eq. (2) are the regular functions or constants.

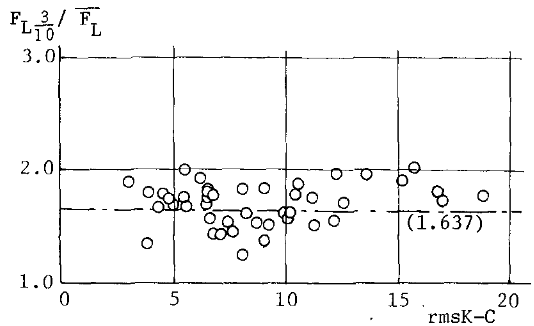

Fig. 10 Ratio of significant lift force to mean lift force versus rmsK-C

Therefore, C_{Ln} must be a random variable. On the other hand, the distribution of the peak lift force is simlor to the Rayleigh distribution from the authors' experiments.[3] Fig.10 shows an example of the relation between the ratio of the significant value of the lift force and its mean value and rmsK-C. The theoretical value of this ratio based on the Rayleigh distribution is 1.637, and it is shown by a strait line in Fig.10. As seen in this figure, the experimental values are scattered around the theoretical value independent of rmsK-C.

Moreover, the lift force spectra in the predominant region of each harmonic lift force component can be considered to be a narrow-band spectra[3),6)]. From the above investigations, the lift force can be assumed to be a random variable of the narrow-band Caussian random process.

Thus, the variance of the lift force can be given by Eq. (3)[7],

$$\sigma_L^2 = E[f_L^2(t)] = \{\frac{1}{2}\rho D U_m\}^2 \ \frac{1}{2}E[C_L^2] \qquad (3)$$

Here, C_L is the lift coefficient of the peak lift force and is a random variable of Rayleigh distribution. Therefor, using the following relation,

$$(C_L)_{rms} = \sqrt{E[C_L^2]} = C_{L1/10}/1.8$$

σ_L is given by Eq. (4) from Eq. (3).

$$\sigma_L = \frac{1}{2}\rho D U_m^2 \left(\frac{C_{L1/10}}{1.8\sqrt{2}}\right) \qquad (4)$$

The validity of Eq.(4) is examined by investigating Eq.(5) deduced from Eq.(4).

$$\sigma_L \Big/ \left(\frac{1}{2}\rho D U_m^2\right) = C_{L1/10}/(1.8\sqrt{2}) \qquad (5)$$

Here, we express the value of the left-hand side of Eq.(5) as ξ, and that of the right-hand side of this equation as ξ'. The value of ξ can be calculated by the standard deviation of the lift force obtained from the measured lift force records. On the other hand, the value of ξ' can also be calculated by using the one-tenth maximum lift coefficient obtained semi-empirically by the authors[3] and is given by Eq.(6) :

$$C_{L1/10} = \begin{cases} 0.245[\text{rmsK-C}] + 0.245 & , \ 0<\text{rmsK-C}<9 \\ -0.155[\text{rmsK-C}] + 3.85 & , \ 9<\text{rmsK-C}<18 \end{cases} \qquad (6)$$

If Eq.(4) is valid, ξ and ξ' have to agree with each other. This agreement of ξ and ξ' is shown in Fig. 11, from which it can be seen that ξ and ξ' agree well regardless of rmsK-C. Therefore, the lift force equation can be expressed as Eq.(7) from Eq.(2) and Eq.(4),

$$f_L(t) = \frac{1}{3.6} C_{L1/10}\, \rho\, D U_m^2 \sum_{n=1}^{4} \frac{S_L(nf_w)\Delta f}{\sigma_L^2} \cos(2n\pi f_w - \theta_n) \tag{7}$$

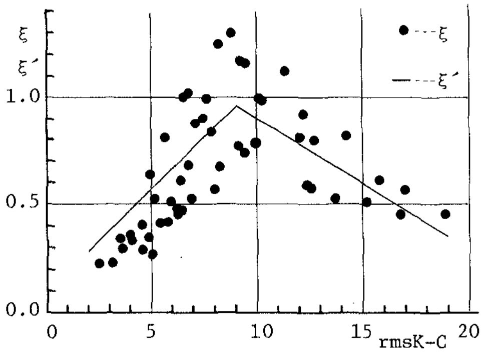

Fig.11 Comparison ξ and ξ' versus rmsK-C

2) EQUATION OF MOTION OF THE PILE

In order to estimate the dynamic response of a single pile structure (see Fig. 1), the pile was idealized by a two-degree of freedom eqivalent spring-mass system with a viscous damper as shown in Fig. 12. The idealization is based on the assumption that the rigidity of the cylinder section on Fig. 1 is much larger than that of the spring bar section, allowing to assume the circular cylinder and the concentrated mass to be a rigid body. In this case, the displacements of the top of pile, X and Y (X and Y are for the X and Y directions respectively), are given by the horizontal displacements at the bottom of the circular cylinder, x and y, and the rotation angles of the circular cylinder, θ_x and θ_y respectively. Furtheremore, assuming $\sin\theta \approx \theta$, X and Y are given by Eq. (8).

$$X = x + L\,\theta_x$$
$$Y = y + L\,\theta_y \tag{8}$$

Here, L : the distance from the bottom of the cylinder to the top of the pile.

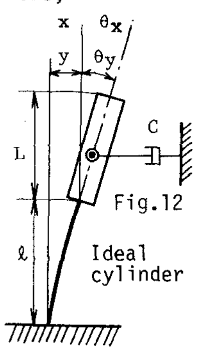

Fig.12 Ideal cylinder

In this study, the mass of the spring bar and the wave force on this bar are assumed to be neglegible, because these values are very small. On these assumptions, the equation of motion of the pile in the X direction due to the in-line force may be given by Eq. (9) and Eq. (10). On the other hand, that in the Y direction may be given by Eq. (11) and Eq. (12). In these equations, it was assumed that the mutual influence between the vibrations of X and Y can be neglected.

$$(m+m_v)\frac{d^2x}{dt^2} + (m+m_v)G\frac{d^2\theta_x}{dt^2} + X\frac{dx}{dt} + G_A C\frac{d\theta_x}{dt}$$
$$+ \frac{6EI}{\ell^3}(2x - \ell\theta_x)$$

$$= \frac{1}{2} C_D \rho D \int_{z_L}^{h+\eta} \left(u - \frac{dx}{dt} - z^* \frac{d\theta_x}{dt}\right) \left|u - \frac{dx}{dt} - z^* \frac{d\theta_x}{dt}\right| dz + \int_{z_L}^{h+\eta} C_M \rho \frac{\pi D^2}{4} \frac{\partial u}{\partial t} dz \tag{9}$$

$$(m + m_V) G \frac{d^2 x}{dt^2} + [I_G + I_{GV} + (m + m_V) G^2] \frac{d^2 \theta_x}{dt^2} + G_A^2 C \frac{d\theta_x}{dt} + \frac{2EI}{\ell^3}(2\ell\theta_x - 3x)$$
$$= \int_{z_L}^{h+\eta} z^* \left[\frac{1}{2} C_D \rho D \left(u - \frac{dx}{dt} - z^* \frac{d\theta_x}{dt}\right) \left|u - \frac{dx}{dt} - \frac{d\theta_x}{dt}\right| + C_M \rho \frac{\pi D^2}{4} \frac{\partial u}{\partial t} \right] dz$$
$$+ \left[mgG_A - \frac{\rho g \pi D^2 (h + \eta - z_L)^2}{8} \right] \theta_x \tag{10}$$

$$(m + m_V) \frac{d^2 y}{dt^2} + (m + m_V) G \frac{d^2 \theta_y}{dt^2} + C \frac{dy}{dt} + G_A C \frac{d\theta_y}{dt} + F_D$$
$$+ \frac{6EI}{\ell^3}(2y - \theta_y) = \int_{z_L}^{h+\eta} f_L(z) dz \tag{11}$$

$$(m + m_V) G \frac{d^2 y}{dt^2} + \{I_G + I_{GV} + (m + m_V) G^2\} \frac{d^2 \theta_y}{dt^2} + G_A C \frac{dy}{dt}$$
$$+ G_A^2 C \frac{d\theta_y}{dt} + M_D + \frac{2EI}{\ell^2}(2\ell\theta_y - 3y)$$
$$= \int_{z_L}^{h+\eta} z^* f_L(z) dz + \left\{ mgG_A - \frac{\rho g \pi D^2 (h + \eta - z_L)}{8} \right\} \theta_y \tag{12}$$

Here, G : distance from the lower end of the cylinder to the center of gravity including the added mass of the cylinder ; G_A : distance from the lower end of the cylinder to the center of gravity minus the added mass of the cylinder ; EI : flexible rigidity of the spring bar ; C : structural damping coefficient ; ℓ : length of the spring bar ; h : still water depth ; η : water surface elevation ; I_G : moment of inertia about the center of gravity due to the total mass minus the added mass of the cylinder ; I_{GV} : moment of inertia about the center of gravity due to the added mass of cylinder ; C_D : drag coefficient ; C_M : mass coefficient ; u : horizontal water particle velocity ; m : total effective mass minus the added mass; m_V : added mass of the cylinder given by Eq.(13).

$$m_V = C_V \pi \rho D\ (h + \eta - z_L)/4 \qquad (13)$$

In Eq.(13), C_V is the coefficient of added mass (C_V=C_M - 1); z_L : distance from the bottom of the water to the lower end of the cylinder; z^*: z-z_L; F_D and M_D are the fluid damping force and moment in the Y direction respectivly, and these are given by Eq. (14) and (15).

$$F_D = \int_{z_L}^{h+\eta} \frac{1}{2} C_D \rho D \left(\frac{dy}{dt} + z^* \frac{d\theta_y}{dt}\right) \left| \frac{dy}{dt} + z^* \frac{d\theta_y}{dt} \right| dz \qquad (14)$$

$$M_D = \int_{z_L}^{h+\eta} \frac{1}{2} C_D \rho d z^* \left(\frac{dy}{dt} + z^* \frac{d\theta_y}{dt}\right) \left| \frac{dy}{dt} + z^* \frac{d\theta_y}{dt} \right| dz \qquad (15)$$

In this analysis, it is assumed that the lift force can be calculated by Eq.(7), and the values of drag and mass coefficients, C_D and C_M, assumes the following values, i.e. C_D=1.5 and C_M=2.2, based on the experimental results of the authors[3].

Since the equations of motion described above are nonlinear differential equations, no exact solution can be obtained. Hence, only approximate solutions can be obtained by using the numerical techniques. In this calculation, Newmark β-method[8] is used to solve the equation of motion. The value of β is selected as 1/6, which is equivalent to a linear acceleration method. The time interval, Δt, is taken as 0.005 sec, because the natural frequency of the second mode of the vibration model ranged from 31 to 35.5Hz for the five kinds of masses shown in Table 1. Taking a stationary response condition into account, the calculation time was as 15 seconds for each case.

3) CALCULATION RESULT

At first, the dynamic displacement in the X direction was computed to investigate the estimation described above (refer to Table 2). Fig. 13 shows a few examples of computation results in the X direction due to the in-line force for values of period ratio about 2 or 3. In this figure, the solid line indicates the calculated result by the method (I), which considers the effect of the finite amplitude nature of the wave, the latter being considered as a sinusoidal wave, on the in-line force, and the dotted line indicates the calculated result by the method (II), which neglects the above-mentioned effect on the in-line force. In other words the integral region of the wave force on the pile is from the lower end of the cylinder to the still water level; η in Eqs.(9) and (10) is assumed to be 0. The measured results are also shown in this figure by small circles.

From this figure, it can be seen that the calculated results by means of method (I) agree well with the measured results. On the other hand, there is much discrepancy in the frequency and magnitude of the displacement between the calculated results by method (II) and the measured results at the period ratio T_w/T_n=2, as shown in Fig. 13 (A) and (B). However, there is little difference between the results of methods (I) and (II) at T_w/T_n=3, as shown in Fig. 13 (C). From this fact, it can be considered that the resonance in the X direction at T_w/T_n=2 is caused by the finite amplitude nature of waves and that at T_w/T_n=3 is caused by the non-linearity of the drag force. Moreover, the dynamic displacement in

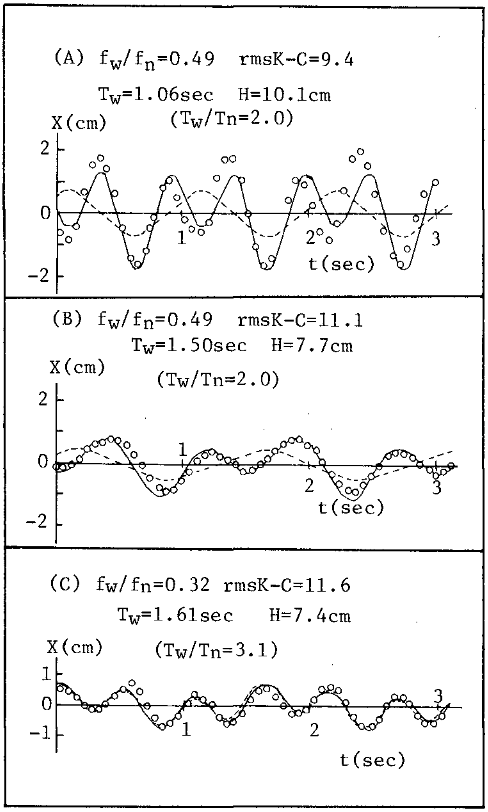

Fig. 13 Calculation results of cylinder displacement in the X direction

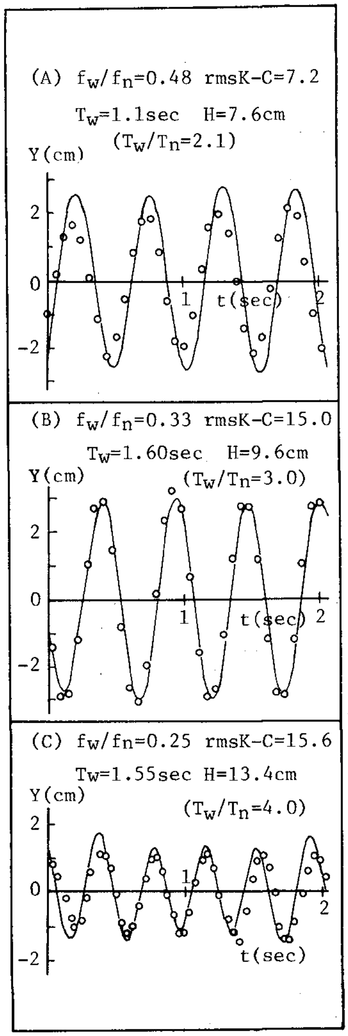

Fig. 14 Calculation results of cylinder displacement in the Y direction

the X direction for other ranges of the period ratio were computed by method (I). As a result, it was confirmed that the dynamic response in the X direction can be calculated by Eqs. (9) and (10) based on method (I) in the range where the period ratio is smaller than 6.5.

Next, the dynamic displacements in the Y direction due to the lift force were also computed by Eqs. (11) and (12) based on method (I) described above. Some examples at the resonance points in the Y direction are shown in Fig. 14. The solid line shows the calculated result and small circles denote the measured result. In this case, as the Y displacement is not regular, the displacement nearly equal to the maximum value is plotted for both the experimental and calculated results.

This figure indicates that the calculated results agree well with the measured results for each resonance point including the properties of the frequency and magnitude of the Y displacements. Therefore, it is concluded that the dynamic response in the Y direction due to the lift force can be calculated by Eqs.(7), (11) and (12).

Finally, the combined dynamic displacements of the pile were computed by composing the calculated displacements in two directions, because the maximum dynamic displacement considering both displacements is desired for an engineering design. Furthermore, comparison between the computed and measured combined dynamic responses gives the whole judgement for the validity of the estimation method of the dynamic responses in both directions. Fig.15 shows this comparison, and the right-hand side of this figure is the calculated result while the left-hand side indicates the measured result. As in Fig. 2, the X-axis is the direction of the wave propagation direction and the Y-axis is the direction normal to the wave propagation direction. Because of the irregularity of the Y displacement, the combined dynamic displacements during one wave cycle in which the maximum combined displacement appears are plotted in Fig. 15. It is apparent that the period raito gradually increases from (A) of $T_w/T_n \approx 1$ ($f_w/f_n \approx 1$) to (G) of $T_w/T_n \approx 5$ ($f_w/f_n \approx 1/5$). A little difference between the measured and calculated locus is observed in the case of (G), in Fig. 15. However, taking into consideration the irregularity of the Y displacement, the calculated results can safely be said to have good agreements with the experimental results. It is concluded that the combined dynamic displacement can be calculated by Eqs.(7), (9), (10), (11) and (12).

CONCLUSION

The dynamic behavior of a fixed circular pile due to the in-line and the lift forces is investigated from the theoretical and experimental stand point of view. It enabled us to arrive at the following conclusions.

First, the resonant responses of a single circular pile due to the lift force in the direction normal to the wave propagation direction are found to take place at the period ratios of T_w/T_n=2,3,4,5 and 6,when rmsK-C is larger than 3. Furthermore, the resonant responses in the wave propagation direction due to the in-line force also appear at the same period ratios as the former case, in addition to the well known resonance at T_w/T_n=1. Moreover, dynamic displacements of the cylinder due to the lift force in the direction normal to the wave propagation direction are larger than those in the wave propagation direction due to the in-line force at the above-mentioned resonance points except at T_w/T_n=1, when rmsK-C is

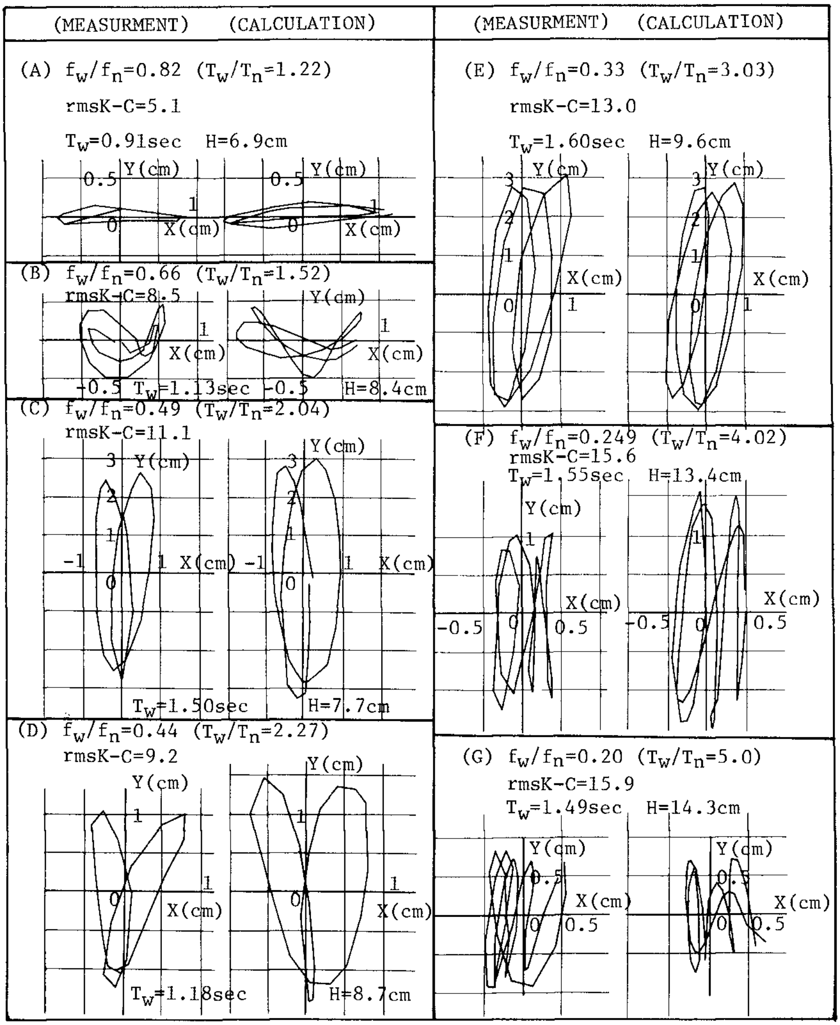

Fig. 15 Calculation results of dynamic loci

larger than 6. Therefore, the lift force is more significant than the in-line force when the natural period of the structure is smaller than the wave period and rmsK-C is comparatively large.

Secondly, the dynamic displacements in both directions and the combined dynamic displacement can be calculated by applying the Morison's formula and the lift force equation to the equation of motion in each direction.

REFERENCES

1) Bidde, D.D.: Laboratory study of lift forces on circular piles, Journal of the Waterways, Harbors and Coastal Engineering Division, ASCE, Vol. 97, No.WW4, 1971, pp. 595-614.
2) Sarpkaya, T.: Forces on rough-walled circular cylinders in harmonic flow, Proc. 15th Conf. on Coastal Engineering, 1976, pp.2301-2330.
3) Sawaragi, T., Nakamura, T. and Kita, H. : Characteristics of lift forces on a circular pile in waves, Coastal Engineering in Japan, vol. 19, 1976, pp.59-71.
4) Wiegel, R.L., Beebe, K.E. and Moon, J. : Ocean wave forces on circular cylindrical piles, Journal of the Hydraulics Division, ASCE, Vol. 83, No. HY2, 1957, pp.1199-1~36.
5) Sarpkaya, T. : Forces on cylinders and spheres in a sinusoidally oscillating fluid, Journal of Applied Mechanics, ASME, Vol. 42, No. 1, 1975, pp.32-37.
6) Chakrabalti, S.K, Wolbelt, A.L. and Tom, W.A. : Wave forces on vertical circular cylinder, Journal of Waterways, Harbors and Coastal Engineering Division, ASCE, Vol. 102, No. WW2, 1976, pp.203-221.
7) Davenport, W.B. Jr and Root, W.L.: An introduction to the theory of random signals and noise, McGraw-Hill Inc., 1958, pp.145-175.
8) Biggs, J.M.: Introduction to structural dynamics, McGraw-Hill,Inc., 1964, pp.1-33.